Atom probe tomography of secondary γ′ precipitation in a single crystal Ni-based superalloy after isothermal aging at 1100 °C

X.P. Tan [a,*], D. Mangelinck [a], C. Perrin-Pellegrino [a], L. Rougier [b], Ch.-A. Gandin [c], A. Jacot [b], D. Ponsen [d], V. Jaquet [d]

[a] IM 2NP, UMR 7334 CNRS, Université Aix-Marseille, 13397 Marseille Cedex 20, France
[b] LSMX, MXG, Ecole Polytechnique Fédérale de Lausanne, 1015 Lausanne, Switzerland
[c] CEMEF, UMR 7635 CNRS, MINES ParisTech, 06904 Sophia Antipolis, France
[d] Snecma-SAFRAN Group, Service YQGC, 92702 Colombes, France

ARTICLE INFO

ABSTRACT

Secondary γ′ precipitation in a commercial single crystal Ni-based superalloy after the 1100 °C isothermal aging has been investigated by atom probe tomography. After the isothermal aging for 300 s, 1800 s and 3600 s, a bimodal size distribution of larger primary γ′ precipitates and numerous smaller secondary γ′ precipitates was obtained. It is proposed that the secondary γ′ precipitated via a non-classical nucleation mode. The coarsening of secondary γ′ precipitates well obeys the classical LSW theory.

© 2014 Elsevier B.V. All rights reserved.

1. Introduction

Commercial single crystal Ni-based superalloy AM1, belonging to the Re-free first generation single crystal Ni-based superalloys, has been extensively used as the materials for high pressure gas turbine blades and vanes in various aircraft engines [1]. As a result of the specific microstructure, e.g. no grain boundary, large amounts of coherent $L1_2$-ordered γ′ precipitates with γ matrix, high γ′ solvus and so on, single crystal Ni-based superalloys have superior high temperature creep properties [2,3]. In particular, their mechanical properties were significantly impacted by the morphology, the size-scale, the volume fraction and the distribution of γ′ precipitation, which mainly rely on the alloying compositions and thermal history [4–6]. The precipitation of γ′ phase has been widely studied in various Ni-based alloys, e.g. Ni–Al–Cr alloys [7–12], polycrystalline superalloys [13–18], single crystal superalloys [19], etc. Atom probe tomography (APT) is a unique and powerful technique, which is able to locate alloying elements and quantify composition at the atomic scale and in the three dimensions [20–23]. It could allow a better understanding of the

γ′ precipitation at a very early stage and the subsequent γ/γ′ interface evolution. Thanks to state-of-the-art local electrode atom probe (LEAP) with faster data acquisition and larger analyzed volume, the investigation on γ′ precipitation was greatly facilitated in single crystal Ni-based superalloys.

Two populations of γ′ precipitation would appear in single crystal Ni-based superalloys via different thermal history, i.e. the primary γ′ precipitation (at high temperature) and secondary γ′ precipitation (at low temperature). Fast cooling rates, such as those undergoing water quench from the high-temperature single γ field, typically lead to the formation of a monomodal size distribution of refined γ′ precipitates. By contrast, slow cooling rates or isothermal annealing would result in the formation of a bimodal size distribution of γ′ precipitates [19]. Furthermore, even a multimodal size distribution of γ′ precipitates (including tertiary γ′) may occur in some cases of polycrystalline superalloys [16]. Recently, different populations of γ′ precipitation in a commercial polycrystalline Ni-based superalloy René 88 DT (processed through powder metallurgy and used in turbine disks) has been systematically investigated by means of APT [15–17,24,25]. Nevertheless, it still lacks of the quantitative composition analysis on different populations of γ′ precipitation in commercial cast single crystal Ni-based superalloys. The secondary γ′ precipitates should be avoided in the commercial single crystal Ni-based superalloys after a standard heat treatment. During the prolonged aging at intermediate

---

* Corresponding author. Current address: NTU Additive Manufacturing Centre (NAMC), School of Mechanical & Aerospace Engineering, Nanyang Technological University, Singapore 639798, Singapore. Tel.: +65 85985452; fax: +65 67919690.
E-mail address: xptan1985@gmail.com (X.P. Tan).

temperatures or creep deformation at elevated temperatures, however, γ channels will widen due to the coarsening of primary γ' precipitates. Numerous secondary γ' precipitates could form inside the widened γ channels. Those finer secondary γ' precipitates are believed to strongly interact with the deformation dislocations and eventually affect the creep properties [26]. In this work, the secondary γ' precipitation via isothermal aging at 1100 °C was investigated by APT.

2. Experimental

As-cast ingots of single crystal Ni-based AM1 superalloy with a composition of Ni–12.15Al–2.41Ta–1.41W–7.15Co–8.55Cr–1.48Ti–1.22Mo (at.%) were provided by SNECMA, (Gennevilliers, France). Solution heat treatment at 1300 °C for 24 h was performed on the single crystal ingots with subsequent air cooling to eliminate chemical segregation. In order to obtain the highest possible cooling rates, thin sections of the solution heat-treated samples (∼1 mm) were solutionized in single γ phase field at 1300 °C for half an hour, followed by a rapid water quench. The cooling rate was estimated to be as high as 1000 °C/s. Isothermal aging heat treatments at 1100 °C for 300 s, 1800 s and 3600 s with subsequent water quench were carried out. The base samples and isothermal aged samples were termed A0, A300, A1800 and A3600, respectively.

APT samples were prepared by cutting $0.2 \times 0.2 \times 20$ mm^3 rods from above-mentioned heat treated samples and by electro-polishing in a 10% perchloric acid in an acetic acid electrolyte at 25–30 V. A fine-polishing was then performed in a 2% perchloric acid in butoxyethanol solution at 5–10 V to form needle-shaped specimens having a radius of curvature of ∼50 nm. APT specimens were analyzed by laser-pulsed local-electrode atom probe (LEAP^{TM}) at 40 K and a gauge pressure $<2 \times 10^{-11}$ Torr. Pulses of green laser light (532 nm wavelength) were applied at a 100 kHz repetition rate with an energy of 0.6 nJ pulse^{-1}, yielding an evaporation rate of 1.20% (∼4 million atoms were collected per hour). Data analysis was performed using IVAS^{TM} 3.6.2 software and compositional information was obtained by employing the proximity histogram (proxigram) methodology [27].

3. Results and discussion

Fig. 1 shows the γ' precipitation evolution after the isothermal aging at 1100 °C for different times. A monomodal size distribution of primary γ' precipitates in A0 sample (Fig. 1a) was obtained by the very high cooling rate. It exhibits the following microstructural features, i.e. irregular morphology of γ' precipitates in the size ranges of ∼30–50 nm, high connectivity of γ' precipitates, diffuse γ/γ' interface, far-from-equilibrium compositions in both γ and γ' phases [28]. After the 1100 °C isothermal aging, a bimodal size distribution of γ' precipitates with larger primary γ' precipitates and numerous smaller secondary γ' precipitates was obtained.
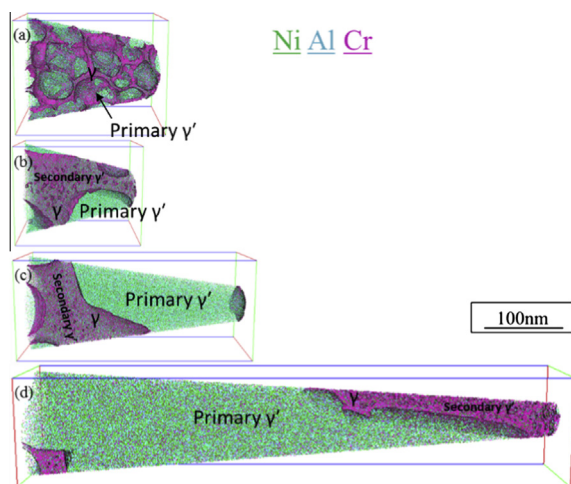

Fig. 1. APT reconstructions showing the γ' precipitates in four AM1 samples (a) A0, (b) A300, (c) A1800 and (d) A3600. 11 at.% Cr iso-concentration surfaces (iso-surfaces) for A0 sample and 12 at.% Cr iso-surfaces for A300, A1800 and A3600 samples were adapted to delineate the γ/γ' interfaces.

Moreover, γ'-free zones with ∼10 nm thick surrounding the primary γ' phase can be clearly seen in A300, A1800 and A3600 samples by the aid of 12 at.% Cr iso-concentration surfaces (iso-surfaces). With the increase of isothermal aging time, the size of primary γ' precipitates was markedly increased. According to the compositions given by the proxigrams in Fig. 2a, all of the alloying elements could be classified into two categories: γ'-forming elements (Al, Ni, Ta and Ti) and γ-forming elements (Cr, Co, Mo and W). Three zones can be defined as illustrated by the Cr concentration profile of A3600 sample in Fig. 2b. The concentration profiles of all elements in the primary γ' phase are flat and remain almost constant with the increasing isothermal aging time. However, there exist obvious concentration gradients in the surrounding γ phase, which correspond to the γ'-free zones. Flat concentration profiles are followed in the secondary γ' and γ coexistence zones. The width of γ'-free zone is found to be ∼7 nm when the primary γ'/γ interface width is taken into account. Moreover, as the isothermal aging time increases, the concentrations of γ-forming elements raise while the concentrations of γ'-forming elements decrease in the secondary γ' and γ coexistence zones. It indicates that the increasing γ-forming elements are rejected from the growing primary γ' precipitates. Since the volume fraction of primary γ' phase is high in AM1 alloy, the compositional variation in the primary γ' phase should be less pronounced in comparison with γ matrix.

In addition to the primary γ' precipitates, a large amount of secondary γ' particles with a high number density and near-spherical shape formed in γ matrix after the isothermal aging at 1100 °C for 300 s, 1800 s and 3600 s (e.g. in Fig. 3). It is worth noting that those secondary γ' precipitates are very small and their precipitation appears able to be prohibited, which is obviously different from the primary γ' precipitation in Fig. 1a. Fig. 4a shows the proxigrams for secondary γ' precipitates in A300, A1800 and A3600 samples. The concentration profiles of all the elements appear to be very similar in A300 and A1800 samples. It means that the precipitation of secondary γ' is likely to enter a steady state during the isothermal aging from 300 s to 1800 s. After the isothermal aging for 3600 s, obvious concentration gradients are revealed in the γ phase surrounding these secondary γ' precipitates for all the elements except for W. It may be due to the low diffusivity of W [3]. The volume fraction of secondary γ' precipitates is relatively low in the secondary γ'/γ coexistence zone, as a result, the compositional variation in the secondary precipitates is remarkable after the isothermal aging for 3600 s. Fig. 4b clearly shows the different zones linked with the secondary γ' precipitates in the proxigrams. A γ phase zone with ∼3.5 nm wide can be defined around the small secondary γ' precipitates, which is much narrower than the γ'-free zones. Due to the existence of concentration gradients in the γ phase around the primary and secondary γ' precipitates, it is not possible to give an accurate composition for γ phase. Table 1 gives the value of the interface width for the primary γ'/γ and secondary γ'/γ interfaces. Table 1 reveals that the primary γ'/γ interface width decreases with the first increasing isothermal aging time. However, it tends to slowly rise for the secondary γ' precipitates. The error bar associated with the interface width is ±0.2 nm based on the bin size used for computing the proxigrams. In addition, the concentration profiles have to be convoluted by a Gaussian function with a full width at half maximum of ∼1 nm [29]. An slight increase in interface width for A3600 sample was attributed to the enhanced concentration gradient in front of γ' precipitates. It is worth noting that the interface widths for both the primary and secondary γ' precipitates in AM1 alloy were substantially larger, corresponding to the compositionally diffuse interfaces, compared to the interface widths from René 88 DT alloy in [24]. It may reveal that the differing precipitation mechanisms act under the different compositions and thermal processes.
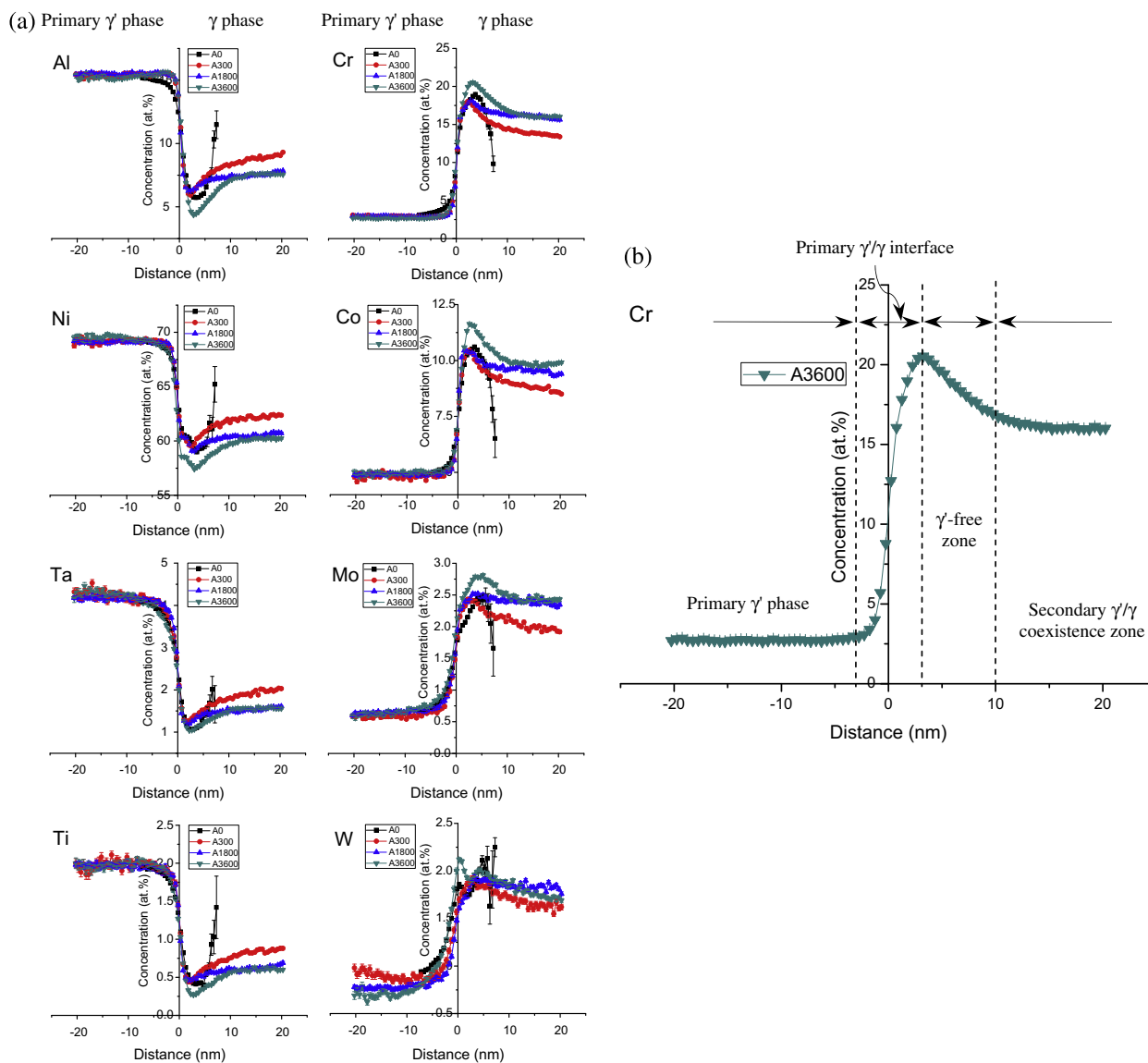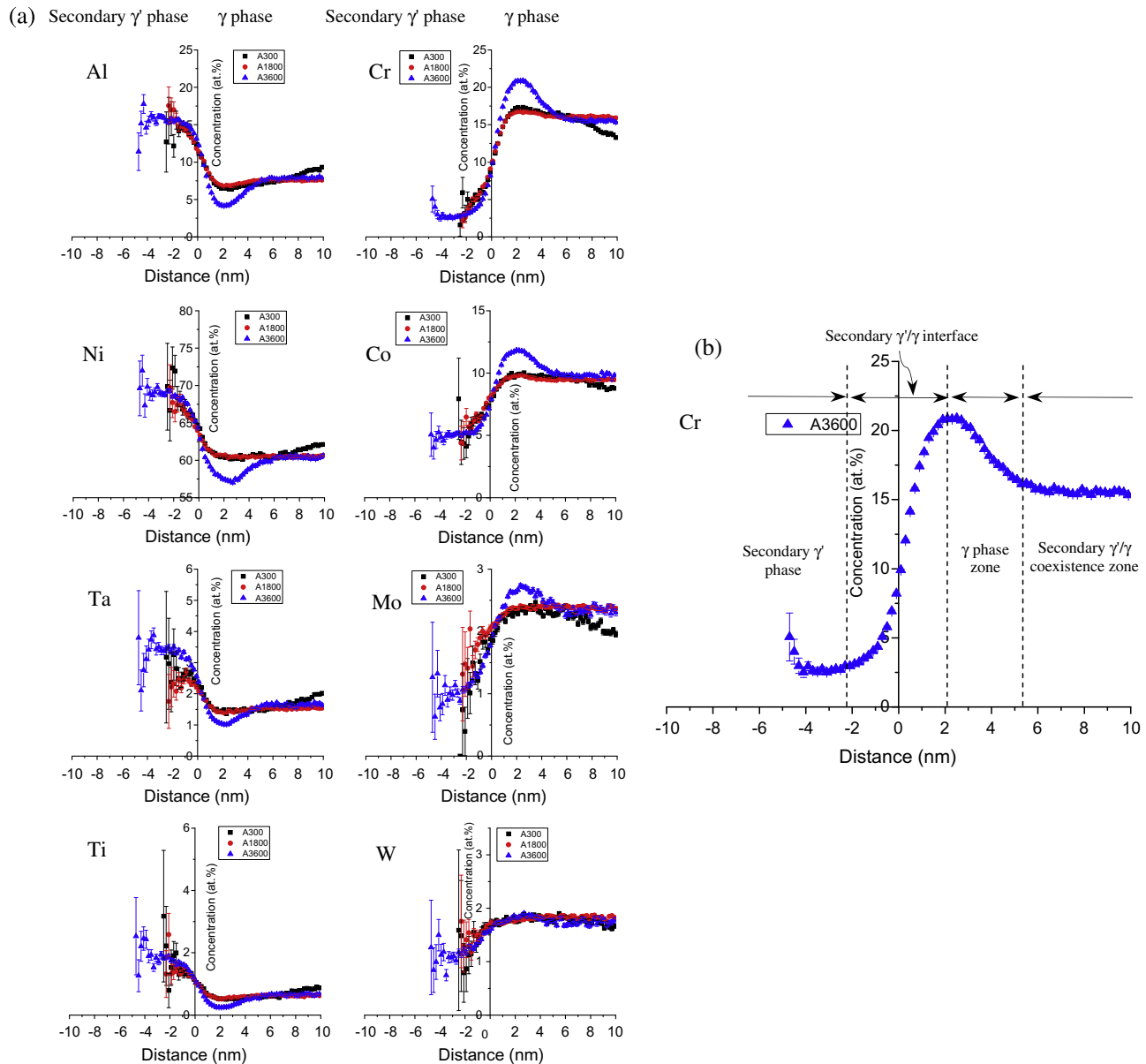
Fig. 2. (a) Proxigrams showing the concentration profiles of all alloying elements across the primary γ′/γ interface delineating with 11 at.% Cr iso-surface in the APT reconstruction of A0 sample and 12 at.% Cr iso-surface for A300, A1800 and A3600 samples. (b) Proxigram of Cr across the primary γ′/γ interface in A3600 sample was adapted to illustrate the different zones.
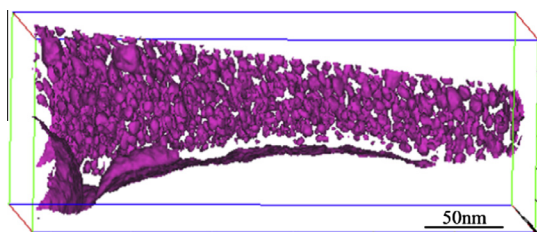
Fig. 3. An APT reconstructed volume showing a large amount of secondary γ′ precipitates in A3600 sample with 12 at.% Cr iso-surfaces.

It has been suggested that the primary γ′ precipitation occurs via a spinodal decomposition when the AM1 alloy was quenched by extremely fast cooling or high undercooling [28]. The supersaturation of secondary γ′/γ coexistence zone should be significantly lower than that in the initial AM1 alloy since the primary γ′ precipitation should have decreased the supersaturation. Unlike the interconnected primary γ′ precipitation at the very early stage,

the secondary γ′ precipitates seem to be mutually separated. In addition, the secondary γ′/γ interface width is significantly narrower than the primary γ′/γ interface. The smallest sizes obtained for the primary and secondary γ′ precipitates are ∼30 nm and ∼1 nm in diameter in AM1 alloy, respectively. That is attributed to the much higher supersaturation in the initial AM1 alloy. Hence, it suggests that the secondary γ′ precipitation mechanism might differ from the primary γ′. As seen in Fig. 4a, furthermore, the secondary γ′/γ interface is diffuse and the concentrations of all elements vary inside the very small secondary γ′ particles, which is in good agreement with the two typical characteristics of non-classical nucleation mechanism [30]. The concentration of γ′-forming elements increasingly raise while γ-forming elements concentration decrease with the increasing isothermal aging time; this indicates that the composition of secondary γ′ precipitates is far-from-equilibrium in the early stage in A300 sample. Based upon the precipitation behavior stated above, it is thus speculated that the secondary γ′ precipitation might take place via a non-classical nucleation mode. However, a more detailed study is required to further prove this precipitation mechanism. As mentioned in

Fig. 4. (a) Proxigrams showing the concentration profiles of all alloying elements across the secondary γ′/γ interface delineating with 11 at.% Cr iso-surface in the APT reconstruction of A0 sample and 12 at.% Cr iso-surface for A300, A1800 and A3600 samples. (b) Proxigram of Cr across the secondary γ′/γ interface in A3600 sample was adapted to illustrate the different zones.

Table 1
The widths of primary γ′/γ and secondary γ′/γ interfaces in the A0, A300, A1800 and A3600 samples.

Sample	Width of primary γ′/γ (nm)	Width of secondary γ′/γ (nm)
A0	6.2 ± 0.2	N/A
A300	4.6 ± 0.2	3.8 ± 0.2
A1800	4.6 ± 0.2	3.8 ± 0.2
A3600	5.2 ± 0.2	4.2 ± 0.2

Booth-Morrison et al. [10], local magnification effects, which may cause some artifacts in the precipitates shape, are not present in the γ/γ′ dual-phase superalloys because the evaporation fields of the two phases are essentially identical. Therefore, the secondary γ′ precipitates size obtained from the APT reconstructed volumes can be considered as reliable. Fig. 5a–c give the size distribution of secondary γ′ precipitates in the three aged samples. Mean radii of the secondary γ′ precipitates in A300, A1800 and A3600 samples are 1.61 ± 0.72 nm, 1.78 ± 0.89 nm and 2.15 ± 1.30 nm,

respectively. Due to the relatively large primary γ′ precipitates and the relatively small analyzed volume by APT, it was not possible to study the coarsening of primary γ′ precipitates. However, the APT technique is suitable for analyzing the coarsening of secondary γ′ precipitation. It has been widely proposed that the coarsening of γ′ precipitates in Ni-based superalloys occurs via Ostwald ripening [15]. Typically, the time-dependent coarsening process is depicted in terms of the LSW model [31,32], i.e.

$$\bar{r}_t^3 - \bar{r}_0^3 = kt, \tag{1}$$

where $\bar{r}_t$ is the mean particle size at a time t, $\bar{r}_0$ is the mean particle size at the onset of coarsening (at $t = 0$), and k is the coarsening constant. Fig. 5d shows that the experimental data appears to fit well with the classical LSW coarsening model expressed by Eq. (1) for the secondary γ′ precipitates. The k value obtained from the slope is 0.0018 nm³ s⁻¹, which is comparable to the values reported in [15] for secondary γ′ precipitates.
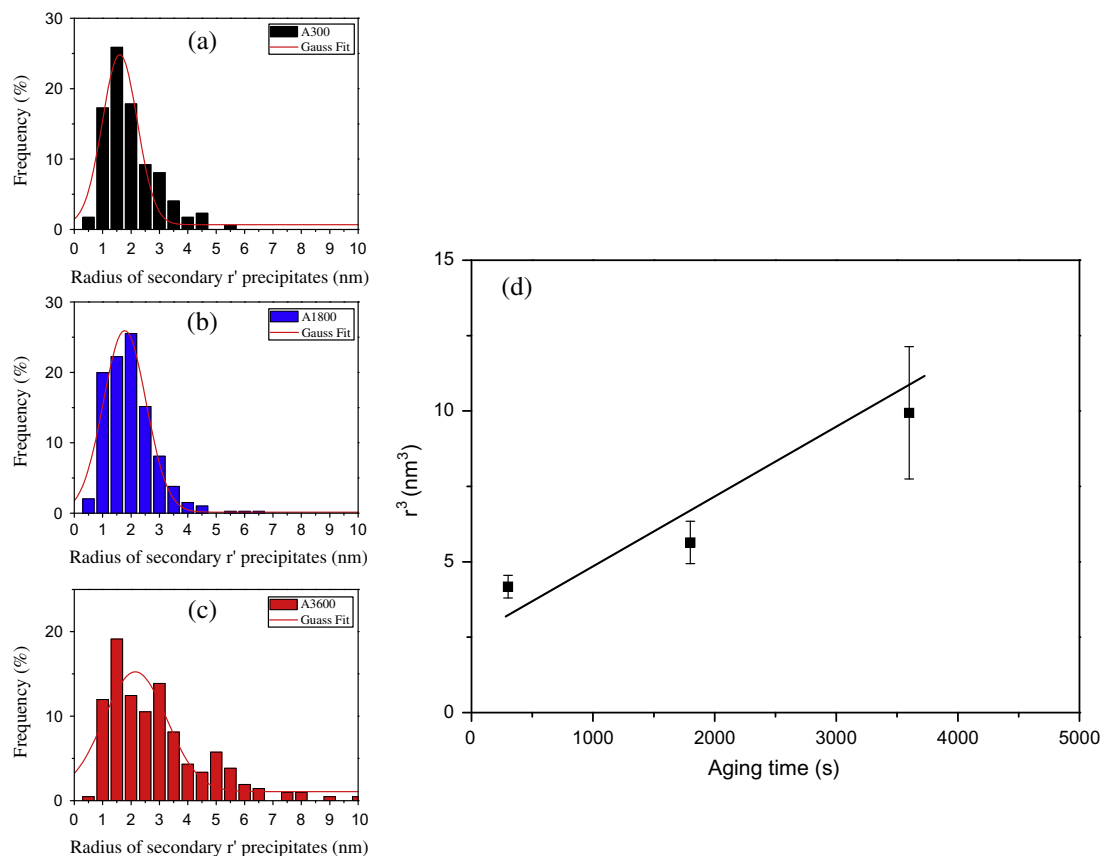
Fig. 5. Size distribution of secondary γ′ precipitates in samples (a) A300, (b) A1800 and (c) A3600. (d) Plot of secondary precipitate size (r^3, in nm^3) vs. aging time (t) after the isothermal aging at 1100 °C. Best linear fit is shown.

4. Conclusions

In summary, a bimodal size distribution of γ′ precipitates with large primary γ′ precipitates and numerous smaller secondary γ′ precipitates was obtained after the isothermal aging at 1100 °C. Different specific zones, i.e. the primary and secondary γ′ phases, the primary and secondary γ′/γ interfaces, the secondary γ′/γ coexistence zone and the γ′-free zone, could be clearly derived in proxigrams. The primary and secondary γ′ precipitates are surrounded by the γ′-free zones with ∼7 nm and ∼3.5 nm widths, respectively. The secondary γ′ precipitation occurs with the following characteristics: diffuse interface, variable composition inside γ′, far-from-equilibrium composition, which suggests a non-classical nucleation process. This possibility needs to be confirmed by further detailed work. The coarsening of secondary γ′ precipitates was found to be in good agreement with the classical LSW model.

References

[1] P. Caron, O. Lavigne, Recent studies at Onera on superalloys for single crystal turbine blades, Aerosp. Lab 3 (2011) 1–14.
[2] M. Durand-Charre, The Microstructure of Superalloys, Gordon and Breach Science Publishers, The Netherlands, Amsterdam, 1997.
[3] R.C. Reed, The Superalloys: Fundamentals and Applications, Cambridge University Press, Cambridge, 2006.
[4] P. Caron, T. Khan, Improvement of creep strength in a nickel-base single-crystal superalloy by heat treatment, Mater. Sci. Eng. 61 (1983) 173–184.
[5] X.P. Tan, J.L. Liu, T. Jin, Z.Q. Hu, H.U. Hong, B.G. Choi, I.S. Kim, C.Y. Jo, Effect of ruthenium on high-temperature creep rupture life of a single crystal nickel-based superalloy, Mater. Sci. Eng., A 528 (2011) 8381–8388.
[6] X.P. Tan, J.L. Liu, T. Jin, Z.Q. Hu, H.U. Hong, B.G. Choi, I.S. Kim, C.Y. Jo, D. Mangelinck, Variation of microstructure by Ru additions in a single crystal Ni based superalloy, Mater. Sci. Technol. 30 (2014) 289–300.
[7] C.K. Sudbrack, K.E. Yoon, R.D. Noebe, D.N. Seidman, Temporal evolution of the nanostructure and phase compositions in a model Ni–Al–Cr alloy, Acta Mater. 54 (2006) 3199–3210.
[8] C.K. Sudbrack, R.D. Noebe, D.N. Seidman, Compositional pathways and capillary effects during isothermal precipitation in a nondilute Ni–Al–Cr alloy, Acta Mater. 55 (2007) 119–130.
[9] C.K. Sudbrack, T.D. Ziebell, R.D. Noebe, D.N. Seidman, Effects of a tungsten addition on the morphological evolution, spatial correlations and temporal evolution of a model Ni–Al–Cr superalloy, Acta Mater. 56 (2008) 448–463.
[10] C. Booth-Morrison, J. Weninger, C.K. Sudbrack, Z. Mao, R.D. Noebe, D.N. Seidman, Effects of solute concentrations on kinetic pathways in Ni–Al–Cr alloys, Acta Mater. 56 (2008) 3422–3438.
[11] C. Booth-Morrison, Y. Zhou, R.D. Noebe, D.N. Seidman, On the nanometer scale phase separation of a low-supersaturation Ni–Al–Cr alloy, Phil. Mag. 90 (2010) 219–235.
[12] Z. Mao, C. Booth-Morrison, C.K. Sudbrack, G. Martin, D.N. Seidman, Kinetic pathways for phase separation: an atomic-scale study in Ni–Al–Cr alloys, Acta Mater. 60 (2012) 1871–1888.
[13] S. Chambreland, A. Walder, D. Blavette, Early stages of precipitation of γ′-phase in a nickel base superalloy: an atom-probe investigation, Acta Metall. 36 (1988) 3205–3215.
[14] S.S. Babu, M.K. Miller, J.M. Vite, S.A. David, Characterization of the microstructure evolution in a nickel base superalloy during continuous cooling conditions, Acta Mater. 49 (2001) 4149–4160.
[15] J. Tiley, G.B. Viswanathan, R. Srinivasan, R. Banerjee, D.M. Dimiduk, H.L. Fraser, Coarsening kinetics of γ′ precipitates in the commercial nickel base Superalloy René 88 DT, Acta Mater. 57 (2009) 2538–2549.
[16] A.R.P. Singh, S. Nag, J.Y. Hwang, G.B. Viswanathan, J. Tiley, R. Srinivasan, H.L. Fraser, R. Banerjee, Influence of cooling rate on the development of multiple generations of γ′ precipitates in a commercial nickel base superalloy, Mater. Charact. 62 (2011) 878–886.
[17] G.B. Viswanathan, R. Banerjee, A.R.P. Singh, S. Nag, J. Tiley, H.L. Fraser, Precipitation of ordered phases in metallic solid solutions: a synergistic clustering and ordering process, Scripta Mater. 65 (2011) 485–488.
[18] A.R.P. Singh, S. Nag, S. Chattopadhyay, Y. Ren, J. Tiley, G.B. Viswanathan, H.L. Fraser, R. Banerjee, Mechanisms related to different generations of γ′

precipitation during continuous cooling of a nickel base superalloy, Acta Mater. 61 (2013) 280–293.

[19] T. Grosdidier, A. Hazotte, A. Simon, Precipitation and dissolution processes in γ/γ' single crystal nickel-based superalloys, Mater. Sci. Eng., A 256 (1998) 183–196.

[20] D. Blavette, E. Cadel, B. Deconihout, The role of the atom probe in the study of nickel-based superalloys, Mater. Charact. 44 (2000) 133–157.

[21] M.K. Miller, Contributions of atom probe tomography to the understanding of nickel-based superalloys, Micron 32 (2001) 757–764.

[22] D.N. Seidman, C.K. Sudbrack, K.E. Yoon, The use of 3-D atom-probe tomography to study nickel-based superalloys, JOM 58 (2006) 34–39.

[23] T.F. Kelly, D.J. Larson, Atom probe tomography 2012, Annu. Rev. Mater. Res. 42 (2012) 1–31.

[24] J.Y. Hwang, S. Nag, A.R.P. Singh, R. Srinivasan, J. Tiley, H.L. Fraser, R. Banerjee, Evolution of the γ/γ' interface width in a commercial nickel base superalloy studied by three-dimensional atom probe tomography, Scripta Mater. 61 (2009) 92–95.

[25] J.Y. Hwang, R. Banerjee, J. Tiley, R. Srinivasan, G.B. Viswanathan, H.L. Fraser, Nanoscale characterization of elemental partitioning between gamma and gamma prime phases in René 88 DT nickel-base superalloy, Metall. Mater. Trans. A 40 (2009) 24–35.

[26] B.C. Wilson, G.E. Fuchs, The effect of secondary gamma-prime on the primary creep behavior of single-crystal nickel-base superalloys, Metall. Mater. Trans. A 41 (2010) 1235–1245.

[27] O.C. Hellman, J.A. Vandenbroucke, J. Rüsing, D. Isheim, D.N. Seidman, Analysis of three-dimensional atom-probe data by the proximity histogram, Microsc. Microanal. 6 (2000) 437–444.

[28] X.P. Tan, D. Mangelinck, C. Perrin-Pellegrino, L. Rougier, C.A. Gandin, A. Jacot, D. Ponsen, V. Jaquet, Spinodal decomposition mechanism of gamma prime precipitation in a single crystal Ni-based superalloy, Metall. Mater. Trans. A (submitted for publication)

[29] H. Benallali, K. Hoummada, M. Descoins, P. Rueda-Fonseca, L. Gerad, E. Bellet-Amalric, S. Tatarenko, K. Kheng, D. Mangelinck, Nature of the ZnSe/GaAs interface investigated by atom probe tomography, Scripta Mater. 69 (2013) 505–508.

[30] R. Wagner, R. Kampann, P.W. Voorhees, in: G. Kostorz (Ed.), Phase Transformation in Materials, WILEY-VCH Verlag GmbH, Weinheim, 2011, p. 341.

[31] I.M. Lifshitz, V.V. Slyozov, The kinetics of precipitation from supersaturated solid solutions, J. Phys. Chem. Solids 19 (1961) 35–50.

[32] C. Wagner, Theorie der Alterung von Niederschlägen durch Umlösen (Ostwald-Reifung), Zeitschrift für Elektrochemie, Berichte der Bunsengesellschaft für physikalische Chemie 65 (1961) 581–591.